A neutron diffraction and ^{27}Al MQMAS NMR study of rare-earth phosphate glasses, $(R_2O_3)_x(P_2O_5)_{1-x}$, $x = 0.187$-0.263, R = Ce, Nd, Tb containing Al impurities

A neutron diffraction and ^{27}Al MQMAS NMR study of rare-earth phosphate glasses, $(R_2O_3)_x(P_2O_5)_{1-x}$, $x = 0.187$–0.263, R = Ce, Nd, Tb containing Al impurities

Jacqueline M Cole†§, Ernst R H van Eck†, Gavin Mountjoy†, Robert J Newport†, Tessa Brennan‡ and George A Saunders‡

† School of Physical Sciences, University of Kent at Canterbury, Canterbury, Kent CT2 7NR, UK
‡ Department of Physics, University of Bath, Claverton Down, Bath BA2 7AY, UK

E-mail: jmc61@cam.ac.uk

Abstract. A neutron diffraction study of four rare-earth phosphate glasses of composition $(R_2O_3)_x(P_2O_5)_{1-x}$, where $x = 0.197, 0.235, 0.187, 0.263$ and R = Ce, Ce, Nd, Tb respectively is presented. The structures of these materials were investigated as a function of (a) rare-earth atomic number and (b) composition. The results show that samples containing the larger rare-earth ions (Ce^{3+} and Nd^{3+}) are coordinated to seven oxygen atoms whereas the immediate environment of Tb^{3+} ions is six coordinate. This implies that rare-earth clustering must be present in the samples containing larger rare-earth ions although no R. . .R correlations are directly observed. Terminal and bridging P–O correlations are resolved, existing in an approximately 1:1 ratio. Second-neighbour O(P)O separations are located with good accuracy and P(O)P correlations relating to the bridging chain are observed. There is also first evidence for the third neighbour correlation, P(OP)O, at $\sim$2.8 Å. A residual feature in the neutron diffraction data, present at $\sim$1.8 Å, is interpreted as Al–O correlations on the basis of ^{27}Al MQMAS NMR experiments. This aluminium impurity originates from the use of aluminium oxide crucibles used in the glass synthesis and is shown to exist as a mixture of octahedral, tetrahedral and penta-coordinated Al–O species. No structural perturbations of the overall network were observed with varying sample composition.

1. Introduction

Rare-earth (R) phosphate glasses with stoichiometries close to those of metaphosphate, $R(PO_3)_3$ and ultraphosphate, RP_5O_{14}, species have shown great promise in the laser and optoelectronics industry. This is because the rare-earth ions possess the required energy levels for achieving successful population inversion and the nonlinear refractive index is large enough to exhibit the desired effects without causing beam breakup and damage. Moreover, the particularly high concentration of rare-earth dopant present in these materials incurs a myriad of exotic physical properties at low temperatures: negative thermal expansion (Acet *et al* 1998), negative pressure dependence of bulk moduli (Mierzejewski *et al* 1988) and unprecedented magnetic, magneto-optical and opto-acoustic phenomena (Carini *et al* 1997).

Despite this multitude of exciting properties, their fundamental structural origins are not well understood. The nature of the atomic structure of these glasses evidently plays an important role in these origins. However, such structural knowledge is sparse, to the extent

§ Author for correspondence. Present address: Department of Chemistry, University of Cambridge, Lensfield Road, Cambridge, CB2 1EW, UK.

that a concerted structural programme is being followed in order to establish a coherent picture of the glass microstructure.

Due to the high structural complexity of glasses, extensive use of a wide range of structural probes is necessary in order to piece together the structure of these materials. Previous work has centred on fluorescence (Farok *et al* 1992, Acet *et al* 1998) and Raman (Mierzejewski *et al* 1988, Lipinska-Kalita *et al* 1995) spectroscopy, EXAFS (Bowron *et al* 1995, 1996, Anderson *et al* 1999) and x-ray diffraction (Bowron *et al* 1995) techniques. The spectroscopic results showed that the rare-earth dopants exist as tripositive ions and are embedded in a phosphate network. The x-ray data confirmed these findings and also revealed that the R^{3+} ions are surrounded exclusively by six to eight oxygen atoms. The corresponding R–O separation ranged from 2.22 to 2.42 Å, depicting classically the lanthanide contraction. P–O correlations were noted in the x-ray diffraction study at 1.55–1.60 Å: typical values for tetrahedral P–O bonds. However, the expected corresponding fourfold coordination of the phosphate group was not entirely apparent. No evidence for any direct R–P or R–R bonding was observed using either technique, the former illustrating that the network is composed exclusively of phosphate groups and the latter denoting that rare-earth clustering was not present at least within a distance of ∼3 Å. The x-ray diffraction study also revealed a second neighbour correlation (O–(P)–O) whilst the EXAFS results intimated the existence of a second neighbour R–(O)–P correlation in the vicinity of 3.1–3.6 Å and one third neighbour correlation, R–(OP)–O in the region of 4.0–4.1 Å.

A combined x-ray and neutron diffraction study on $(La_2O_3)_{0.253}(P_2O_5)_{0.747}$ glass has also been reported (Hoppe *et al* 1998). This investigation revealed that the P–O correlation resolves into two overlapping peaks, split in a 1:1 ratio and situated at distances of 1.48 and 1.60 Å. The split relates to two different types of P–O bond: those at the shorter distance that have terminal (π-bonded) oxygen atoms (corresponding to P–O. . .R correlations, denoted P–O_T) and those at the longer distance that have bridging (σ-bonded) oxygen atoms (corresponding to P–O–P bonding, denoted P–O_B). Their existence in a 1:1 ratio is indicative of an entirely Q^2 phosphate network (where Q^n is the number of oxygen atoms which branch from a given cation—in this case, phosphorus) which concurs with the structure of the $La(PO_3)_3$ crystal analogue (Matuszewski *et al* 1988). However, the nature of the immediate rare-earth environment differs between the crystal and the glass: in the crystal, the R^{3+} ion lies in a distorted eightfold oxygen coordinated site whereas a coordination number, $N_{RO} = 7.1(5)$ was deduced from the investigation by Hoppe *et al* (1998) on the glass. The reliability of this value is good, despite the obscuring peak due to the O–(P)–O correlation because the different atomic scattering factors between x-rays and neutrons allow a good contrast of peak intensities between the two data-sets. A coordination number of seven implies that the LaO_7 polyhedra cluster via a bifurcated interaction of O_T to two La ions, since only O_T atoms are expected to coordinate to the rare-earth ion. No direct evidence of clustering in terms of La–(O_T)–La correlations was reported, although no correlations beyond 3 Å were modelled.

Since lanthanum is the largest of all the lanthanides, the sequential decrease in size of the rare-earth ion across the lanthanide series may induce significant structural perturbations both in the immediate rare-earth environment and in the phosphate network. Such perturbations may include marked changes in the minimum R. . .R separation, knowledge of which is particularly important industrially since the optical and magnetic properties of these glasses are severely impaired by rare-earth clustering. This, coupled with the desire to look at structural alterations due to changes in composition, provided the impetus for the investigation reported herein.

This study expands upon the aforementioned neutron diffraction work in the form of a neutron diffraction investigation of four further rare-earth phosphate glasses and includes complementary ^{27}Al NMR results which focus on the consequences of the sample fabrication

method. The samples chosen for study were $(R_2O_3)_x(P_2O_5)_{1-x}$ where R = Ce, Ce, Nd, Tb and $x = 0.197, 0.235, 0.187, 0.263$ respectively. The selection of these particular rare earths resulted from a careful interplay of obtaining large ion size differences whilst ensuring that the rare earth possessed a significant nuclear scattering cross-section, low nuclear absorbance and a minimum number of Breit–Wigner nuclear resonances within the energy region of interest. Cerium was the optimal rare earth in terms of its nuclear properties and so was the sample chosen for making a direct comparison of compositional change. The high contrast in composition between a near-ultra- and near-metaphosphate glass of the respective neodymium and terbium samples is expedient for investigating concurrent compositional and rare-earth ion size changes.

2. Experiment

2.1. Sample preparation and characterization

The samples were prepared by heating 25 mol% of the high purity (99.9%) grade rare-earth oxide in the presence of excess P_2O_5 in an aluminium oxide crucible at a temperature corresponding to the rare-earth oxide melt (1400–1650 °C). Full synthetic details are described by Mierzejewski *et al* (1988). The extreme synthetic thermal conditions, to some degree, make it difficult to attain exact compositional precision. However, it is possible to synthesize such compounds within the compositional region of meta- and ultraphosphate. The rare earth concentrations in the resulting samples were deduced by electron probe microanalysis.

2.2. Neutron diffraction experiments

The neutron diffraction experiments were performed on the Liquids and Amorphous Diffractometer (LAD) at the ISIS facility of the Rutherford Appleton Laboratory, Chilton, Oxfordshire, UK which employs the time-of-flight technique. The finely powdered samples were placed in a 6 mm diameter cylindrical vanadium can and placed in the centre of the vertically cylindrical instrument. Data were collected over a period of 1800–3000 μA h using detector groups positioned on the periphery of the instrument at scattering angles, 5, 10, 21, 35, 58, 90 and 148°, both to the left and to the right of the 1.5 cm (width) × 3.5 cm (height) incident beam. This yielded data across 14 ranges of the scattering vector, Q, where $|Q| = (4\pi \sin\theta)/\lambda$, 2θ is the scattering angle and λ is the incident neutron wavelength. A vanadium rod was used to record the primary energy spectrum of the neutron source and thence remove it from the data. Data were also collected on an empty 6 mm diameter vanadium can and used to subtract sample container contributions from the sample spectra. All data were normalized, corrected and merged in a standard fashion using the ATLAS suite of programs (Hannon *et al* 1990). Nuclear resonances were present in several of the neodymium and terbium data sets. These features were removed from the data by simply limiting the Q_{max} in the given detector bank to the maximum unaffected value of Q (as determined by comparing the data with that from separate unaffected detector banks). A significant amount of paramagnetic scattering was also present in the terbium data. The theoretical paramagnetic contribution of Tb^{3+} ions to the differential cross-section was therefore calculated, using the following equation (Bacon 1975) which assumes a perfect paramagnet, and removed from the merged data.

$$\Delta\sigma/d\Omega = 2/3g^2 J(J+1)/4(e^2\gamma/mc^2)f(s)^2.$$

$\Delta\sigma/d\Omega$ is the differential scattering cross-section, g is the Landé splitting factor ($g = 1 + [J(J+1) + S(S+1) - L(L+1)]/2J(J+1)$), e is the electronic charge (in cgs units), γ is the magnetic moment of a neutron in Bohr magnetons, m is the electron mass, c is the speed

of light (in cm s^{-1}), $s = (\sin\theta)/\lambda$ and f is the magnetic form factor which was calculated according to the spin-only and first order orbital contribution:

$$f(s) = \langle j_0(s) \rangle + (1 - 2/g)\langle j_2(s) \rangle.$$

$\langle j_0(s) \rangle$ and $\langle j_2(s) \rangle$ are spherical Bessel functions calculated according to Brown (1995). Contributions from higher order terms are expected to be negligible (Steinsvoll *et al* 1967).

The resultant interference functions, $i(Q)$ (Gaskell 1991) extended up to $Q_{max} = 50\,\text{Å}^{-1}$; oscillations were observable up to this limit and were Fourier transformed according to:

$$t(r) = 2\pi^2 r\rho_0 + \int_{Q_{min}}^{Q_{max}} Q i(Q) \sin(Qr)\,\mathrm{d}Q$$

where r is the atomic separation between atoms, $t(r)$ is the atomic pairwise distribution function and ρ_0 is the atomic density.

Atomic pair functions were then simulated in reciprocal space according to the equation (Gaskell 1991):

$$p_{ij}(Q) = N_{ij}(w_{ij}/c_j)(\sin(QR_{ij})/QR_{ij})(\exp(-Q^2\sigma_{ij}^2/2)$$

where $p_{ij}(Q)$ is the pair function in reciprocal space, N_{ij}, R_{ij} and σ_{ij} are the coordination number, atomic separation and thermal parameter of atom i with respect to j, c_j is the composition of atom j and w_{ij} is the weighting function of atoms i and j which follows the relation:

$$w_{ij} = (2c_i b_{i,coh} c_j b_{j,coh})/\bar{b}_{coh}^2 \qquad \text{where } i \neq j$$

or

$$w_{ij} = (c_i b_{i,coh})^2/\bar{b}_{coh}^2 \qquad \text{where } i = j.$$

Initial estimates of the values of R_{ij}, N_{ij} and σ_{ij} for each pair function were made based on the features present in the experimental $t(r)$ curve and each pair function was converted into $t(r)$ via a Fourier transform according to the equation:

$$t(r) = \int_0^{Q_{max}} Q p_{ij}(Q) \sin(Qr)\,\mathrm{d}Q.$$

The R_{ij}, N_{ij} and σ_{ij} parameters were then refined iteratively and the procedure above repeated until the sum of the Gaussian models gave a good fit to the experimental curve.

2.3. Monte Carlo modelling

A Monte Carlo method was also used to obtain a $t(r)$ function by fitting directly to the experimental $i(Q)$ data. This yields a $t(r)$ profile which exhibits the minimum deviation from the gas-like underlying curve that is also consistent with the $i(Q)$ to within its error; it thus represents a close analogy to a 'maximum entropy' inversion of $i(Q)$. The MCGR program (Pusztai and McGreevy 1997) was used to accomplish this with the parameters $\Delta Q = 0.02\,\text{Å}^{-1}$, $Q_{max} = 50\,\text{Å}^{-1}$, $\Delta r = 0.05\,\text{Å}$, $r_{max} = 20\,\text{Å}$, $\sigma_E = 0.01$ and the constraint $t(r) = 0$ for $r < 1.35\,\text{Å}$.

2.4. ^{27}Al NMR experiments

The ^{27}Al NMR experiments were performed on a CMX Infinity 300 solid-state NMR spectrometer at a magnetic field strength of 7.05 T using a 4 mm HX MAS probe which was resonant at 78.233 MHz for ^{27}Al. The octahedral resonance of YAG was used as an external reference for aluminium at 0.7 ppm, which also served to determine the RF field
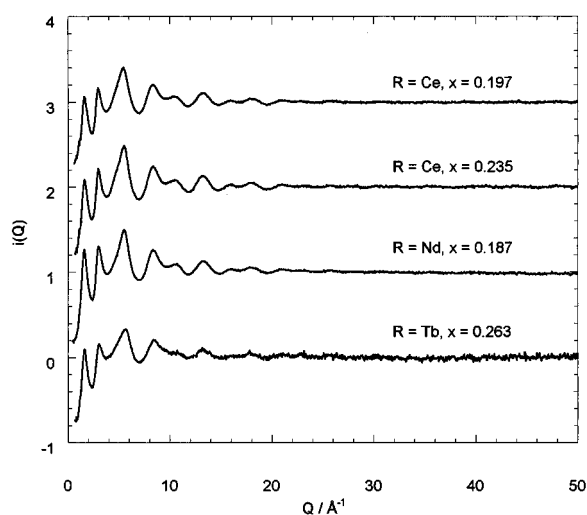
Figure 1. Interference functions for $(R_2O_3)_x(P_2O_5)_{1-x}$, R = Ce, Ce, Nd, Tb; $x = 0.197, 0.235,$ 0.187, 0.263 respectively.

strength. All spectra were acquired at a magic angle spinning speed of 15 kHz. Single pulse spectra were acquired with an RF-field strength of 80 kHz, using a 0.8 μs pulse.

^{27}Al triple quantum 2D MQMAS (two dimensional multiple quantum magic angle spinning) experiments (Frydman and Harwood 1995, Smith and van Eck 1999) were performed on all samples. The MQMAS experiment correlates the $\langle 1/2, -1/2 \rangle$ transition with the symmetric $\langle m, -m \rangle$ multiple quantum transition of non-integer quadrupolar nuclei ($I = 5/2$ and the $\langle 3/2, -3/2 \rangle$ transition in our case). This results in a high resolution two dimensional spectrum where resonances that overlap in a 1D MAS spectrum are usually resolved in the 2D spectrum. From the position of a peak in a 2D MQMAS spectrum one can determine the isotropic shift, which is the same for both dimensions, and the quadrupole induced shift (QIS), which is different for the single and triple quantum transitions. The QIS provides an upper and lower limit for C_q, the quadrupole coupling constant.

For the MQMAS experiments the Z-filter pulse sequence was employed (Amoureux *et al* 1996, Dirken *et al* 1997). An RF field strength of 140 kHz was used for the excitation and conversion pulses of 3.05 and 1.25 μs, respectively. Phase sensitive detection in the triple quantum dimension was done using TPPI.

3. Results

Figure 1 shows that the $i(Q)$ for each of the samples is of good quality overall. The terbium interference function is slightly noisier than the others which is a consequence of the small sample mass available: the sample covered vertically only 7 mm of the 35 mm high beam. The corresponding experimental and modelled $t(r)$ functions for each sample are given in figure 2 together with the appropriate MCGR fit. All three $t(r)$ functions are in good agreement with each other in each case. An illustration of the manner in which the individual Gaussian peaks combine to form this total t(r) model is given in figure 3 using the example of $(Ce_2O_3)_{0.197}(P_2O_5)_{0.803}$. A total of seven Gaussian peaks were fitted to the experimental $t(r)$ profile in each case. Table 1 lists the nature of these correlations along with their atomic separation, R, coordination number, N, and Debye–Waller factor, σ^2. The model was applied

Table 1. Atomic separations, R_{ij}, coordination numbers, N_{ij} and Debye–Waller factors, σ_{ij}^2, for each modelled atomic pairwise correlation in $(R_2O_3)_x(P_2O_5)_{1-x}$, where R = Ce, Ce, Nd, Tb and x = 0.197, 0.235, 0.187 and 0.263 respectively.

Rare earth	Atomic number	Comp, x	PO_T			PO_B			RO		
			N	R	σ^2	N	R	σ^2	N	R	σ^2
Ce	58	0.197(5)	1.8(4)	1.49(1)	0.003(1)	1.8(4)	1.60(1)	0.005(1)	6.0(6)	2.42(2)	0.008(1)
Ce	58	0.235(5)	1.9(4)	1.49(1)	0.001(1)	1.9(4)	1.60(1)	0.003(1)	5.8(6)	2.43(2)	0.006(1)
Nd	60	0.187(5)	1.9(4)	1.49(1)	0.002(1)	1.8(4)	1.60(1)	0.004(1)	5.3(6)	2.39(2)	0.008(1)
Tb	65	0.263(5)	1.7(4)	1.49(1)	0.002(1)	1.9(4)	1.60(1)	0.006(1)	5.8(6)	2.27(2)	0.015(2)

Rare earth	Atomic number	Comp, x	O(P)O			P(OP)O		
			N	R	σ^2	N	R	σ^2
Ce	58	0.197(5)	3.4(3)	2.50(1)	0.007(2)	4.0(5)	2.82(3)	0.017(5)
Ce	58	0.235(5)	3.4(3)	2.50(1)	0.006(2)	3.8(5)	2.81(3)	0.020(5)
Nd	60	0.187(5)	3.3(3)	2.49(1)	0.006(2)	4.6(5)	2.78(3)	0.030(5)
Tb	65	0.263(5)	3.4(3)	2.50(1)	0.009(2)	5.1(5)	2.86(3)	0.025(5)

Rare earth	Atomic number	Comp, x	P(O)P			O(R)O		
			N	R	σ^2	N	R	σ^2
Ce	58	0.197(5)	2.8(9)	3.02(4)	0.007(2)	3.2(5)	3.23(3)	0.017(5)
Ce	58	0.235(5)	2.9(9)	3.01(4)	0.005(2)	3.1(5)	3.24(3)	0.020(5)
Nd	60	0.187(5)	2.5(9)	3.01(4)	0.003(1)	3.2(5)	3.24(3)	0.017(5)
Tb	65	0.263(5)	2.0(9)	3.00(4)	0.008(2)	2.9(5)	3.22(3)	0.012(5)

up to a distance of $\sim$3.5 Å, beyond which the preponderance of many intense, overlapping P–O correlations precluded any further unambiguous modelling. In the range modelled, the experimental $t(r)$ profile is emulated very well, except in the vicinity of 1.8 Å. The residual feature present at 1.8 Å also appeared in the MCGR results and therefore is not simply an artefact of Fourier inversion. A consideration of ionic radii would suggest that this weak feature is associated with a low level of aluminium impurity in the sample (electron probe microanalysis showed a level of 1–2 wt.% Al).

The ^{27}Al NMR spectrum for the lanthanum phosphate glass (figure 4, note that La^{3+} is diamagnetic) shows three peaks that might originate from three different sites. These features are not resolvable in the other glasses due to paramagnetic broadening; one should also note that the aluminium spectra for the paramagnetic glasses differ in their degree of broadening, not only between the neodymium and cerium glasses but also between the two different cerium compositions. To investigate the impurity aluminium environment further, multiple quantum magic angle spinning (MQMAS) NMR spectra were recorded on all accessible samples (La, Ce (x = 0.197, 0.235) and Nd). Figure 5 displays the triple quantum ^{27}Al 2D MQMAS spectra of the lanthanum glass (top) and one of the cerium glasses (x = 0.197, bottom). The three features present in the single pulse ^{27}Al spectrum of the lanthanum sample are now well resolved into three separate peaks, indicating three different aluminium environments. Based on the estimated centre of gravity, the isotropic chemical shift and the quadrupole interaction can be determined for each peak (see table 2). The ^{27}Al MQMAS spectrum of the cerium phosphate glass does not resolve the broad peak into constituent peaks. However, paramagnetic broadening will affect both dimensions, obscuring any separate contributions. The broad peak covers the same range as the three separate peaks for the lanthanum glass,
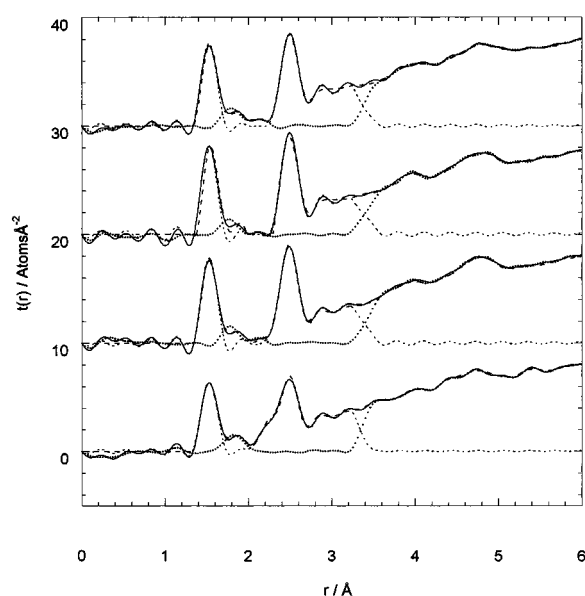
Figure 2. $t(r)$ profiles for $(R_2O_3)_x(P_2O_5)_{1-x}$, R = Ce, Ce, Nd, Tb; x = 0.197, 0.235, 0.187, 0.263 respectively. The solid, short dashed, dotted and long dashed lines represent the experimental, model, residual and MCGR fit respectively.

Table 2. The isotropic chemical shifts and quadrupolar coupling constants of $(La_2O_3)_{0.225}(P_2O_5)_{0.775}$, calculated on the basis of an estimated centre of gravity.

Peak number	δ_{iso} (ppm)	C_q max ($\eta = 0$) (MHz)	C_q min ($\eta = 1$) (MHz)
1	39.8	3.7	3.2
2	9.9	3.3	2.9
3	−17.6	2.8	2.4

giving a strong indication that the same three aluminium species are present in this cerium glass as in the lanthanum glass (such coincidences can also be seen for the other two glasses).

The existence of more than one type of Al–O correlation in the lanthanum sample suggests that aluminium oxide from the crucible enters the reaction melt and that at least some of this impurity is incorporated into the network (phase separated Al_2O_3 would yield only one peak). Such an impurity level has been observed previously in other metal phosphate glasses (Abrahams *et al* 1997, Hartmann *et al* 1994). Moreover, the expected atomic separations of such multiple Al–O correlations observed in the ^{27}Al NMR study match those of the residual peak at ∼1.8 Å in the neutron diffraction study.

4. Discussion

4.1. The rare-earth environment

The R_{RO} separations illustrate the lanthanide contraction as expected and the R_{LaO} distance (2.458(15) Å) obtained by Hoppe *et al* (1998) conforms well with this series as shown in figure 6. The R_{TbO} value determined here supports very well the value obtained from previous EXAFS results from the same sample (2.267(5) Å) (Bowron *et al* 1995) whereas EXAFS
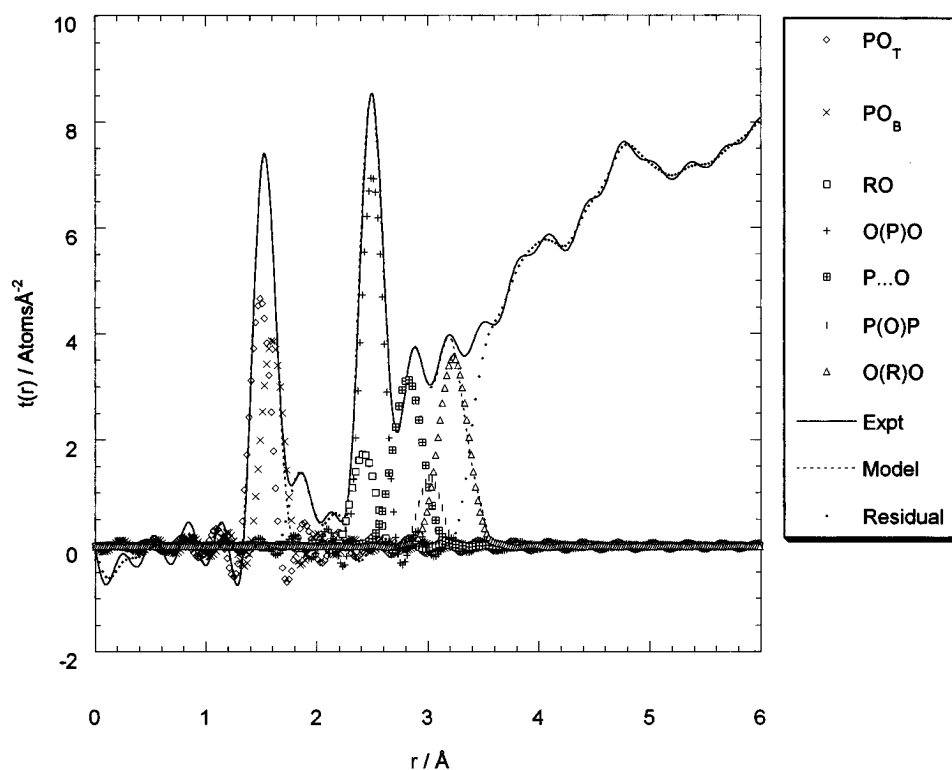
Figure 3. An illustration of the modelling of individual atomic correlations via the example $(Ce_2O_3)_{0.197}(P_2O_5)_{0.803}$.

derived R_{CeO} and R_{NdO} distances (2.35(1) and 2.34(1) Å respectively) from Ce ($x = 0.235$) and Nd ($x = 0.187$) samples (Anderson *et al* 1999) are slightly lower than those reported herein. However, more credence is given to the neutron derived values since double-electron excitations were present in the EXAFS data of the cerium and neodymium samples which are known to cause inaccuracies within the fitting process (D'Angelo *et al* 1996).

The R_{RO} values may be compared with tabulated ionic radii of six-, seven- and eightfold coordinated R^{3+} ions (Shannon 1976), from which coordination numbers of 7, 7 and 6 for the cerium, neodymium and terbium samples respectively are implied (see figure 6). This contrasts with the coordination number, N_{RO}, of approximately 6 obtained directly from the model fit for each sample. However, the accuracy of this parameter is questionable since another peak of much greater intensity, corresponding to the near-equidistant O(P)O correlation, heavily obstructs the RO peak, thereby reducing the reliability of the modelled area.

The constant nature of the $R_{O(R)O}$ separations further corroborates the evidence towards sevenfold coordination in the phosphate glasses with larger rare-earth ions: R_{RO} and R_{ORO} distances relate to average ORO angles of 84(3), 84(3), 85(3) and 90(3)° for the Ce ($x = 0.197$), Ce ($x = 0.235$), Nd and Tb samples respectively. Thus, the Tb^{3+} ion appears to be octahedral on average whilst the acute angles in the other cases imply the presence of an extra oxygen atom. The value of σ_{RO} for the terbium sample is also significantly larger than for the cerium and neodymium ones, therefore suggesting it has a more disordered local environment.

A corollary to this sevenfold coordination is the existence of rare-earth clustering: bridging oxygen atoms are not expected to participate in R...O coordination and so one terminal oxygen
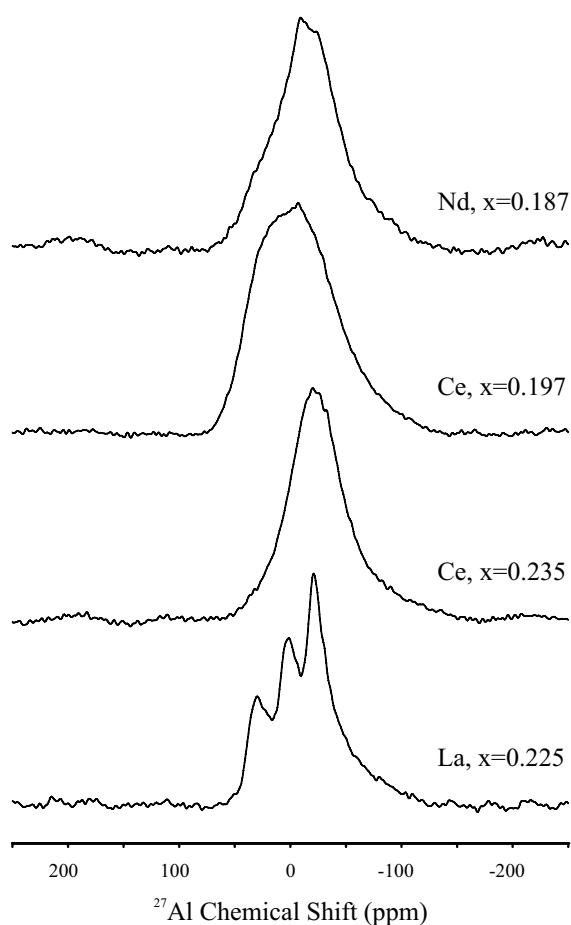
Figure 4. ^{27}Al single pulse spectra of four rare-earth phosphate glasses containing an aluminium impurity.

atom must be coordinated to two rare-earth ions in a bifurcated fashion. No evidence for any R. . .R correlations was found in the cerium or neodymium data although this is not surprising since the low scattering cross-sections of the rare-earth elements result in weak correlations which are heavily overshadowed by the dominant P. . .O contributions to the $t(r)$ distribution in the spatial region of interest ($\sim$4–6 Å). Attempts are currently under way in order to ascertain the minimum R. . .R separation through anomalous x-ray and neutron diffraction studies since this technique enables one to separate the R. . .X contributions from all other pairwise correlations.

4.2. The phosphate network

The PO_T and PO_B correlations were readily resolved and modelled for each sample, yielding R_{PO_T} and R_{PO_B} separations of 1.49(1) and 1.60(1) Å. These values are fully consistent with expectations for the fourfold nature of the phosphate group. Moreover, they compare very well to those deduced for the analogous lanthanum material (Hoppe *et al* 1998). Expected ratios for N_{PO_T} and N_{PO_B} are 2:2 and 1.6:2.4 for meta- and ultraphosphate networks respectively. The values of N_{PO_T} and N_{PO_B} reported herein (see table 1) agree with these expected ratios within experimental error but are not sufficiently accurate for discerning effects of composition on
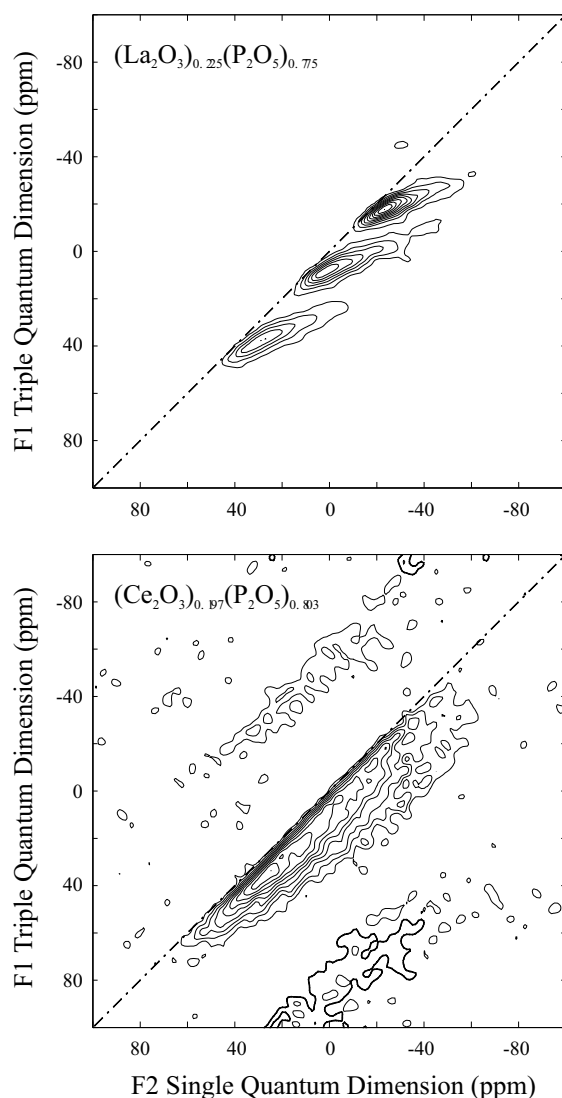
Figure 5. ^{27}Al triple quantum 2D MQMAS spectra of $(La_2O_3)_{0.225}(P_2O_5)_{0.775}$ (top) and $(Ce_2O_3)_{0.197}$ $(P_2O_5)_{0.803}$.

the phosphate network. The values of σ_{PO_B} are significantly larger than σ_{PO_T} as observed by Hoppe *et al* (1998) for the lanthanum metaphosphate glass.

Second neighbour O(P)O correlations were also observed for each compound with separations between 2.49 and 2.50(1) Å and with a coordination number ranging from 3.3(3) to 3.4(3). The reliability of the $R_{O(P)O}$ values was very good, as deduced by evaluating the OPO angle using the $R_{O(P)O}$ values in conjunction with the mean R_{PO} distance (1.545 Å): values of 107.4–108.0° were obtained which are within experimental error of the necessary 109.5° average required for tetrahedral geometry. The coordination numbers, $N_{O(P)O}$, are all within three standard deviations of the expected values of 4.00–4.07, the lower and upper limits corresponding to values for the metaphosphate and ultraphosphate compositions. These expectations were calculated according to the following argument: six O(P)O correlations
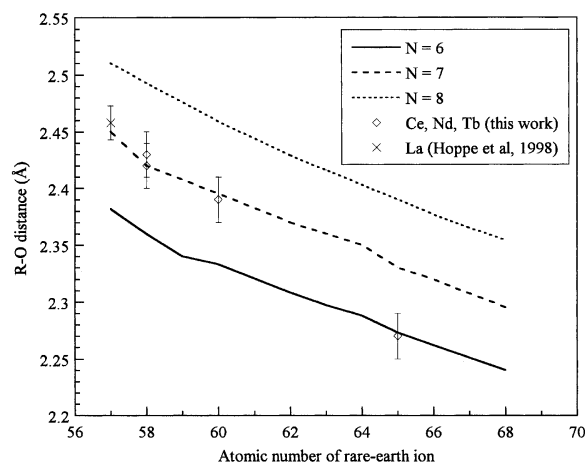
Figure 6. The variation of R_{RO} with rare-earth ionic size. The lines on the plot represent the values expected for R–O distances calculated from tables of ionic radii of R^{3+} ions (Shannon 1976) with coordination numbers of 6 (solid line), 7 (long dashed line) and 8 (short dashed line).

emanate from a bridging oxygen atom whereas only three originate from a terminal oxygen atom; the metaphoshate, $R(PO_3)_3$, has a P:O ratio of 1:3 and so two bridging:two terminal oxygen atoms are present per phosphorus atom (bridging bonds are shared and therefore each count as half an oxygen); this totals to $1/3$ of the oxygen atoms having an O(P)O coordination of 6 and $2/3$ having an O(P)O coordination of 3, i.e. 4.0 on average. In the ultraphosphate (RP_5O_{14}) limit, a P:O ratio of 1:14/5 exists and so there are one bridging:1.8 terminal oxygen atoms which totals to $5/14$ oxygen atoms involved with six O(P)O correlations and $9/14$ oxygen atoms involved with three O(P)O correlations, i.e. 4.07 on average.

The chain component of the phosphate network is apparent through a small peak corresponding to P(O)P correlations. The model gave identical $R_{P(O)P}$ and $N_{P(O)P}$ values for each compound within experimental error: 3.00(4)–3.02(4) Å and 2.0(9)–2.9(9) respectively. The large errors reported here reflect the difficulty in modelling these correlations due to the overlapping of other peaks to either side which are much more intense since they correspond to correlations involving elements with combined nuclear cross-sections markedly greater than that of phosphorus. The values of $N_{P(O)P}$ are consistent with both meta- and ultraphosphate species (2 and 2.5 respectively). Calculations using the $R_{P(O)P}$ and R_{PO_B} separations were made in order to determine the POP angle. This yielded values of 139.3(14)–141.4(14)° which compares with a mean POP angle of 137 and 134° calculated from all reported analogous meta- and ultraphosphate crystal structures respectively (Tranqui *et al* 1972, 1974, Hong, 1974a, b, Jezowska-Trzebiatowski *et al* 1980, Dorokhova and Karpov 1984, Rzaigui *et al* 1984, Matuszewski *et al* 1988, Cole *et al* 1999).

One previously unobserved type of correlation was also located. Its intense nature precluded rare-earth ions or solely phosphorus atoms from being responsible for its presence and an O...O correlation was ruled out since the combined nuclear cross-section of oxygen is far too large. By process of elimination, the peak must therefore be due to a P...O correlation. Indeed, a P...O model fits well, yielding realistic parameters: $R_{P...O} \approx 2.8$ Å, $N_{P...O} = 3.8(5)$–5.1(5) and $\sigma^2_{P...O} = 0.017(5)$–0.030(5) Å^2. The most likely origin of this P...O correlation is the fragment P(OP)O.

Various other third (and higher) neighbour phosphate correlations at larger distances

continue to form the remainder of the $t(r)$ profile. However, their broad and numerous distributions (due to the free rotation permitted about the P–O σ-bonds) precludes any possibility of modelling them.

4.3. Structural effects with change in composition

No change in the rare-earth or phosphate environment with varying composition could be detected from the neutron data. The distinct structural differences observed between meta- and ultraphosphate crystals (Hong 1974a) suggest however that structural perturbations with varying composition may well occur in the glasses over this range of atomic correlation. Hence, it is either the case that the glasses retain a metaphosphate-like structure at all intermediate compositions (as would be suggested on the basis of optical data (Farok *et al* 1992)) or that a mixture of local environments is present, which alters to allow a more or less gradual change. Either way, neutron diffraction alone is not capable of discerning this. ^{31}P NMR investigations are currently under way in order to try to further probe this question.

4.4. Sample fabrication: consequential Al incorporation

A distinct residual peak is present in each $t(r)$ profile at $\sim$1.8 Å. No realistic correlation involving any combination of rare-earth, phosphorus or oxygen atoms could be modelled at this distance. Moreover, such a peak was not present in the $La(PO_3)_3$ neutron diffraction study (Hoppe *et al* 1998). The origin of this weak feature was explored via ^{27}Al NMR studies. The chemical shifts of $\sim$40 and ~ -18 ppm and their associated coupling constants (see table 2) are indicative of tetrahedral and octahedral Al–O sites with phosphorus in the second coordination shell respectively whereas the origin of the peak at 9.9 ppm is unclear. The three possible responsible features are: octahedral $Al(OAl)_6$ (Dupree *et al* 1985), $Al(OR)_6$ (Hartmann *et al* 1994) or a penta-coordinated phosphorus environment (Brow *et al* 1993, van Eck *et al* 1995). The latter option is the favoured possibility here since (i) phase separation is unlikely since the two other peaks show that aluminium is incorporated into the network and (ii) the chemical shift of this peak does not vary from sample to sample despite the differing paramagnetic strengths of the rare-earth ions.

The octahedral aluminium sites presumably form in environments analogous to those containing rare-earth ions. The tetrahedral aluminium sites are probably those normally filled with phosphorus atoms and so some charge balancing is required. Such balancing may be achieved via a greater phosphorus or lower oxygen content. The variation in the relative amounts of tetrahedral aluminium present between samples is intriguing: the near-ultraphosphate composition samples ($R = Ce$, $x = 0.197$ and $R = Nd$, $x = 0.187$) showed the weak presence of tetrahedral aluminium sites whereas the cerium sample containing a greater rare-earth content ($x = 0.235$) gave no evidence for tetrahedral aluminium at all. However, further corroborative evidence is required, and this is the subject of future work.

These results also explain why no residual feature at $\sim$1.8 Å was observed in the $La(PO_3)_3$ study (Hoppe *et al* 1998) since in that case a platinum crucible was used for the glass synthesis. Preliminary synthetic investigations on similar glasses using a platinum crucible show that such samples are noticeably more brittle and fragile. This suggests that the 1–2 wt.% of aluminium present in the samples reported herein physically strengthens the phosphate network. Further work on sample fabrication is currently under way in order to clarify this issue.

5. Conclusions

This neutron diffraction study reveals seven atomic correlations, two of which relate to the rare-earth environment whilst the other five correspond to the phosphate network. R_{RO} values reproduce the lanthanide contraction, compare well with the previous neutron diffraction study (Hoppe *et al* 1998) and are representative of a seven-coordinate rare-earth environment for the cerium and neodymium samples, falling to six-coordinate for the terbium sample. Thus, the immediate rare-earth environment is dependent on the rare-earth ionic size. A corollary to the seven-coordinate rare-earth environment is rare-earth clustering. However, no evidence for any R...R correlations was observed, presumably because the preponderance of intense P...O correlations in the region where R...R correlations are expected precluded this. Bridging and terminal P-O bonding was distinguished and second neighbour O(P)O correlations were determined with good accuracy. The phosphate chain was also detected through P(O)P correlations and one previously unobserved correlation, P(OP)O, was here observed. A residual peak at ∼1.8 Å was assigned to Al–O correlations following a ^{27}Al NMR investigation. About 1–2 wt.% Al, originating from the aluminium oxide crucible used in the sample fabrication, appears to be incorporated in the glass network in three different environments: octahedral, tetrahedral and probably penta-coordinated. The neutron results showed no evidence of any overall structural change to the network with varying glass composition.

Acknowledgments

References

Abrahams I, Franks K, Hawkes G E, Philippou G, Knowles J, Bodart P and Nunes T 1997 *J. Mater. Chem.* **7** 1573
Acet M, Brennan T, Cankurtaran M, Saunders G A and Zähres H 1998 *Phil. Mag.* B **77** 1633
Amoureux J P, Fernandez C and Steuernagel S 1996 *J. Magn. Reson.* A **123** 116
Anderson R, Brennan T, Cole J M, Mountjoy G, Pickup D M, Newport R J and Saunders G A 1999 *J. Mater. Res.* **14** at press
Bacon G E 1975 *Neutron Diffraction* 3rd edn (Oxford: Clarendon) p 259
Bowron D T, Newport R J, Rainford B D, Saunders G A and Senin H B 1995 *Phys. Rev.* B **51** 5739
Bowron D T, Saunders G A, Newport R J, Rainford B D and Senin H B 1996 *Phys. Rev.* B **53** 5268
Brow R K, Kirkpatrick R J and Turner G L 1993 *J. Am. Ceram. Soc.* **76** 919
Brown P J 1995 *International Tables for Crystallography* vol C, ed A J C Wilson (Dordrecht: Kluwer) pp 391–5
Carini G, D'Angelo G, Tripodo G, Fontana A, Rossi F and Saunders G A 1997 *Europhys. Lett.* **40** 435
Cole J M, Lees M R, Howard J A K, Newport R J, Saunders G A and Schönherr E 1999 *J. Solid State Chem.* submitted
D'Angelo P, Pavel N V, Roccatano D and Nolting H-F 1996 *Phys. Rev.* B **54** 12 129
Dirken P J, Kohn S C, Smith M E and van Eck E R H 1997 *Chem. Phys. Lett.* **266** 568
Dorokhova G I and Karpov O G 1984 *Sov. Phys. Crystallogr.* **29** 400
Dupree R, Farnan I, Forty A J, El-Mashri S and Bottyan L 1985 *J. Physique Coll.* **46** C8
Farok H M, Saunders G A, Poon W and Vass H 1992 *J. Non-Cryst. Solids* **142** 175
Frydman L and Harwood J S 1995 *J. Am. Chem. Soc.* **117** 5367
Gaskell P H 1991 *Materials Science and Technology* vol 9, ed J Zrzycky (Weinhaim: VCH) ch 4
Hannon A C, Howells W S and Soper A K 1990 *(IOP Conf. Ser. 107)* (Bristol: Institute of Physics) p 193
Hartmann P, Vogel J and Schnabel B 1994 *J. Non-Cryst. Solids* **176** 157
Hong H Y-P 1974a *Acta Crystallogr.* B **30** 468
——1974b *Acta Crystallogr.* B **30** 1857
Hoppe U, Kranold R, Stachel D, Barz A and Hannon A C 1998 *J. Non-Cryst. Solids* **232–234** 44
Jezowska-Trzebiatowski B, Mazurak Z and Lis T 1980 *Acta Crystallogr.* B **36** 1639

Lipinska-Kalita K E, Fontana A, Leonardi A, Carini G, D'Angelo G, Tripodo G and Saunders G A 1995 *Phil. Mag.* **71** 571

Matuszewski J, Kropiwnicka J and Znamierowski T 1988 *J. Solid State Chem.* **75** 285

Mierzejewski A, Saunders G A, Sidek H A A and Bridge B 1988 *J. Non-Cryst. Solids* **104** 323

Pusztai L and McGreevy R L 1997 *Physica* B **234** 357

Rzaigui M, Kbir Ariguib N, Averbuch-Pouchot M T and Durif A 1984 *J. Solid State Chem.* **52** 61

Shannon R D 1976 *Acta Crystallogr.* A **32** 751

Smith M E and van Eck E R H 1999 *Prog. NMR Spectrosc.* **34** 159–201

Steinsvoll O, Shirane G, Nathans R, Blume M, Alperin H A and Pickart S J 1967 *Phys. Rev.* **161** 499

Tranqui D, Bagieu M and Durif A 1974 *Acta Crystallogr.* B **30** 1751

Tranqui D, Bagieu-Beucher M and Durif A 1972 *Bull. Soc. Fr. Mineral. Crystallogr.* **95** 437

van Eck E R H, Kentgens A P M, Kraus H and Prins R 1995 *J. Phys. Chem.* **99** 16 080